Do seasonal forecasts of Indian summer monsoon rainfall show better skill with February initial conditions?

K. Rajendran[1,2,*], Sajani Surendran[1,2], Stella Jes Varghese[2] and Arindam Chakraborty[3]

[1]Multi-Scale Modelling Programme, CSIR Fourth Paradigm Institute, Bengaluru 560 037, India
[2]Academy of Scientific and Innovative Research, Ghaziabad 201 002, India
[3]Centre for Atmospheric and Oceanic Sciences; and DST Centre for Excellence in Climate Change, Divecha Centre for Climate Change, Indian Institute of Science, Bengaluru 560 012, India

Prediction for Indian summer monsoon rainfall (ISMR) is generated by integrating model from initial conditions (ICs) of weather at some time prior to season. We examine the factors responsible for the widely reported highest ISMR forecast skill for February ICs in climate forecast system (CFSv2) model. Skill for February ICs is highest only based on correlation between observed and predicted year-to-year variation of ISMR, whereas other skill scores indicate highest skill for late-April/early-May ICs having shorter yet useful forecast lead-time. Higher correlation for February ICs arises from correct forecasting of 1983 ISMR excess, which is however due to wrong forecast of La Niña and correlation drops to lower value than that for late-April/early-May ICs if 1983 is excluded. Forecast skill for sea-surface temperature variation over equatorial central Pacific (ENSO) in Boreal summer is lowest for February ICs indicating role of dynamical drift induced by long forecast lead-time. Model deficiencies such as oversensitivity of ISMR to ENSO and unrealistic ENSO influence on variation of convection over equatorial Indian Ocean (EQUINOO) lead to errors in ISMR forecasting. In CFSv2, ISMR is mostly decided by ENSO whereas in observation it is influenced by ENSO and EQUINOO independently.

RAINFALL received over India during the summer season (June–September, JJAS) is known as the Indian summer monsoon rainfall (ISMR). There has been considerable year-to-year variation (interannual variation, IAV) in the quantum of ISMR that has a profound effect on the agricultural sector and the socio-economic well-being of the country. Hence, it is essential to predict ISMR or its departure in a season correctly to facilitate effective planning of agricultural and economic strategies, and water and hydel power management. In spite of the challenges in modelling the Indian summer monsoon due to its complex features and multiple processes involved, coupled ocean–atmosphere general circulation models (CGCMs) have become an essential tool for dynamical seasonal prediction[1]. The climate forecast system version 2 (CFSv2) model of the National Centers for Environmental Prediction (NCEP), USA, is an outcome of such efforts in recent years to improve dynamical prediction, and its forecast skill is widely studied[2–6]. Recently, this model has been adopted by the Ministry of Earth Sciences, Government of India, for dynamical seasonal prediction of the Indian summer monsoon.

Over the tropics, the existence of slowly varying boundary conditions constitutes the basic premise of seasonal prediction[7]. Anomalous IAV of sea-surface temperature (SST) over the equatorial central Pacific associated with El Niño-Southern Oscillation (ENSO)[8], is considered to be the primary source of predictability[9]. Krishnamurthy and Shukla[10] examined the predictability of ISMR in eight CGCMs, including CFS for forecast and predictability errors and estimated the doubling time of errors for rainfall over India, to be 4–14 days in the CFS against 4–7 days in other models. Forecast skill will improve as the initial conditions (ICs) get closer to the prediction period, and thus the highest forecast skill is expected for ICs with 0-month lead time (L0). In other words, the skill is expected to increase (decrease) with decreasing (increasing) lead time when considering the development of dynamical shift in the model with time[11] and systematic biases caused due to deficient representation of physical processes in the model. Kumar et al.[12] analysed the CFS forecast skill of monthly mean SST and precipitation, and showed that the skill rapidly reduces with lead time. After a lead time of about 30–40 days, the forecast skill for monthly mean was found to reduce, with SST anomalies in the tropical central/eastern Pacific playing a dominant role. Thus, for seasonal predictability, the conditions of the ocean state also become important. They suggested the reduction in skill is due to the large contribution

from the atmospheric internal variability to monthly means[12].

Contrary to expectation and the understanding of significant ENSO spring predictability barrier and low predictability of ENSO forecasts during February and March[13], CFSv2 predictions of ISMR with February ICs (three-month lead time, L3), were reported to have the maximum forecast skill[14–17], based on the correlation between observed and predicted IAVs of ISMR during the analysis period. Further, the skill scores reported in previous studies vary considerably among themselves depending upon (i) the region selected for averaging the summer season rainfall to estimate ISMR for each year, (ii) the reference dataset used as observation, and (iii) duration of the analysis period. These seasonal forecast verifications were performed with datasets rarely exceeding 29 samples, which can also lead to highly uncertain scores[18]. However, an understanding of the impact of different ICs on ISMR forecast skill is fundamental and central to improving its predictability. Thus, it is imperative to understand what contributes to the forecast skill of February (L3) ICs. We focused on the factors which influence ISMR variability in CFSv2 by comparing its seasonal reforecasts (hindcasts) with observations/reanalyses, with emphasis on its dependence on SST boundary forcing. We analysed large datasets of CFSv2 reforecasts initialized with ICs starting from January to May, which were made available by NCEP. To reconfirm major results and to understand the advantage of choosing ICs which are nearer to the forecast period (JJAS) yet having useful lead time, we assessed the performance skill of the current version of CFSv2 by analysing its reforecasts initialized with an optimum subset of five late-April/early-May (hereafter referred to as Late-L1/Early-L0) ICs.

Model, seasonal reforecasts, datasets and methodology

CFSv2 is a coupled dynamical forecast system with global forecast system model in triangular truncation of T126 (~0.9375° horizontal resolution) having 64 hybrid sigma-pressure levels as the atmospheric component and Geophysical Fluid Dynamics Laboratory Modular Ocean Model (GFDL MOM4) with 0.25° horizontal resolution in the equatorial region (±10° lat.) and 0.5° elsewhere as the ocean component[5].

To examine the dependence of ISMR forecast skill of CFSv2 on ICs, we analysed 124 nine-month retrospective seasonal reforecasts or hindcasts (hereafter referred to as 'CFSv2–NCEP') initiated from CFS reanalysis based ICs on every fifth day starting from 1 January (four-month forecast lead time, L4) to 31 May (0-month lead time, L0), with four reforecasts per day (at 00, 06, 12, 18 UTC) during 1982–2010 (ref. 2). These datasets were made

available by NCEP in their web portal (https://www.ncdc.noaa.gov/data-access/model-data/model-datasets/climate-forecast-system-version2-cfsv2). We analysed month-wise CFSv2–NCEP seasonal reforecasts initiated with 28 L4 (January), 20 L3 (February), 24 L2 (March), 24 L1 (April) and 28 L0 (May) ICs, during 1982–2010.

We carried out a set of nine-month reforecasts for the analysis period, initiated from 5 ICs with short lead times in late-April (Late-L1), viz. 00 UTC of 21 and 26 April, and early-May (Early-L0) viz. 00 UTC of 1, 6 and 11 May, using the current version of CFSv2 (which is being employed for seasonal prediction as the monsoon mission model by Ministry of Earth Sciences, Government of India), at the computing platform of Council for Scientific and Industrial Research (CSIR) Fourth Paradigm Institute, Bengaluru (hereafter referred to as 'CFSv2–CSIR'). There are no differences in the physics or numerics documented between CFSv2–NCEP and CFSv2–CSIR, except for minor bug-fixings[5] and possible differences due to changes in the computing platform. Our analysis of retrospective forecasts revealed that the bias in representing the spatial distribution of climatological summer mean monsoon rainfall over India reduces with May ICs. The skill scores of correlation between the observed and predicted IAVs of ISMR during 1982–2010 were also found to be comparatively better for the ensemble means of April and May ICs. This led us to chose an optimum subset of five above-mentioned late-April/early-May (Late-L1/Early-L0) ICs, which were close to the onset of the monsoon season yet having reasonable and useful lead time. These ICs yielded better skill scores in forecasting IAV of ISMR. For performing a set of experimental reforecasts which generate large outputs for about three decades, we had optimized the number of ICs to five which can yield the best skill score, i.e. two late-April and three early-May ICs. These runs were analysed to verify major results on the forecast skill for ISMR and boreal summer-time ENSO, in the current version of the model. The major results were re-verified using CFSv2–NCEP reforecasts with the same five late-April/early-May (Late-L1/Early-L0) ICs.

For validation, $0.25 \times 0.25°$ gridded India Meteorological Department (IMD) rainfall[19], Global Precipitation Climatology Project (GPCP) version 2.3 data[20] and Hadley Centre Ice and SST (HadISST) data[21] were used. Daily optimum interpolation SST version 2.1 (OISSTv2.1 at $0.25° \times 0.25°$ horizontal resolution) data were also analysed[22]. For validation of 850 hPa winds, we used fifth generation European Centre for Medium Range Weather Forecast Reanalysis (ERA5) data[23]. NINO3.4 (170°–120°W; 5°S–5°N) SST anomaly (normalized by standard deviation) was used as ENSO index. The ENSO index >1 (<1) indicates El Niño (La Niña). It is important to note that our analysis focused on ENSO during the Indian summer monsoon season (i.e. JJAS). Negative of the anomaly of surface zonal wind at the equatorial Indian
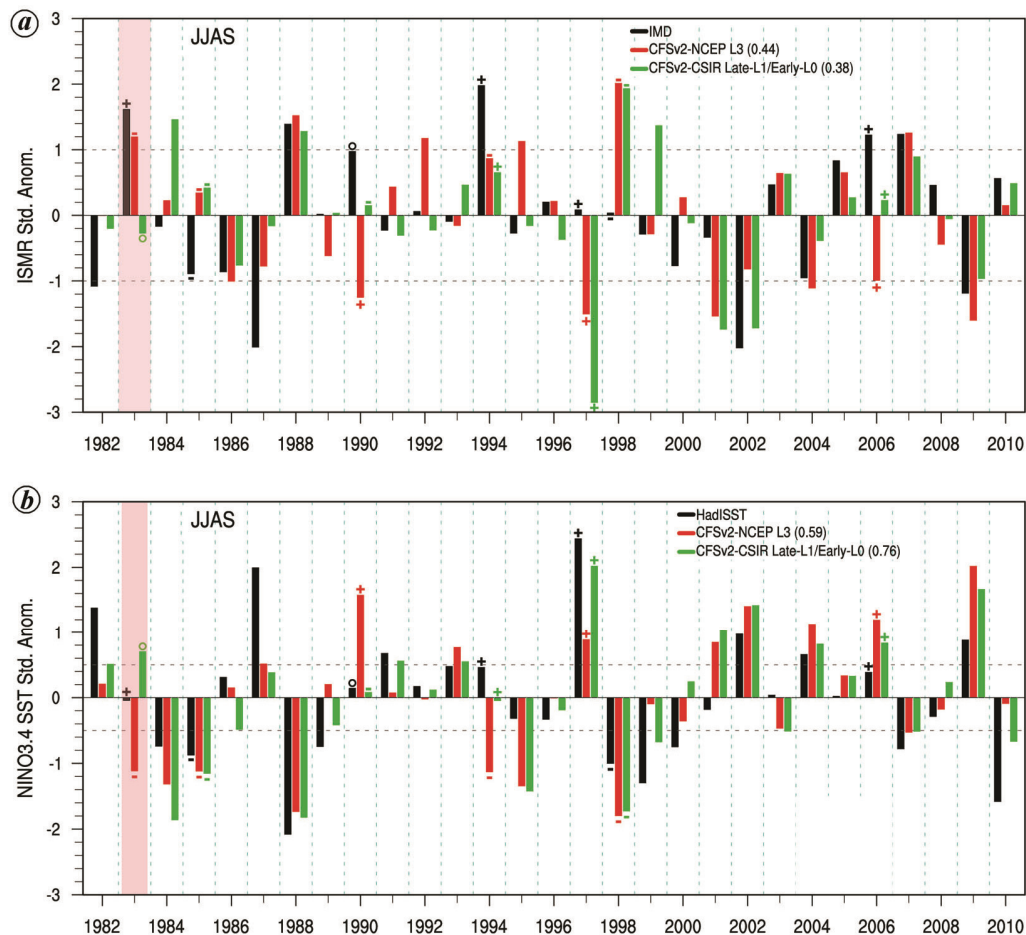
Figure 1. *a*, Interannual variability (IAV) of standardized anomalies of Indian summer monsoon rainfall (ISMR) over the monsoon region predicted by the ensemble mean of CFSv2–NCEP L3 reforecasts and CFSv2–CSIR Late-L1/Early-L0 reforecasts, compared with the IAV of ISMR anomalies from India Meteorological Department (IMD) observations. The 1983 anomalies are highlighted in light red background colour. *b*, Same as (*a*) but for anomalies of ENSO index defined as standardized anomalies of NINO3.4 sea-surface temperature (SST). Positive, negative and neutral anomalies of the EQUINOO index for special years of 1983, 1985 1990, 1994, 1997, 1998 and 2006 are represented by '+', '−' and 'o' respectively.

Ocean (IO, 60°–90°E; 2.5°S–2.5°N) estimated from ERA5, was used as the index for equatorial Indian Ocean oscillation (EQUINOO)[24].

For estimating seasonal mean ISMR for each year, we used the rainfall averaged over the monsoon region[25]. Anomalies of ISMR and indices of ENSO and EQUINOO were standardized with their standard deviation. For assessing the performance of forecasting IAV of ISMR, basic skill scores such as ISMR temporal mean, standard deviation and coefficient of variation (CV) were used. Deterministic skill scores such as mean error, bias and root mean square error (RMSE) were also used. Appendix 1 provides details of these methods.

ISMR forecast skill dependence on initial conditions

Figure 1 *a* shows the IAV of standardized ISMR anomalies from IMD observations and deterministic ensemble means of CFSv2–NCEP L3 and CFSv2–CSIR Late-L1/Early-L0 reforecasts for 1982–2010. Correlation coefficients (γ) between observed ISMR anomalies and those from the ensemble means of CFSv2–NCEP reforecasts with L4, L3, L2, L1, L0, and CFSv2–CSIR reforecasts with Late-L1/Early-L0 ICs were 0.26, 0.44, 0.27, 0.35, 0.25 and 0.38 respectively. Based on the Fisher r to z transformation, these correlations were not significantly different from each other.

It can be seen that the correlation-based ISMR forecast skill is the highest for CFSv2–NCEP L3 ($\gamma = 0.44$) followed by CFSv2–NCEP L1 ($\gamma = 0.35$) ICs. It is important to note that the performance of ensemble mean of CFSv2–CSIR Late-L1/Early-L0 reforecasts ($\gamma = 0.38$, Figure 1 *a*) is better than the skill of ensemble mean of CFSv2–NCEP reforecasts with other ICs, except L3. In fact, its correlation skill is higher than that of the ensemble mean of CFSv2–NCEP reforests with five Late-L1/Early-L0 ICs which is 0.35 (shown in Figure 2).

Figure 1 *b* shows the corresponding IAV of boreal summer ENSO index (NINO3.4 SST) anomalies. Correlation coefficients between observed HadISST-based ENSO index anomalies and those from the ensemble means of CFSv2–NCEP reforecasts with L4, L3, L2, L1, L0, and CFSv2–CSIR reforecasts with Late-L1/Early-L0 ICs were 0.59, 0.59, 0.64, 0.74, 0.80 and 0.76 respectively. The correlations increased for later ICs. ISMR excess of 1983 in L3 was associated with erroneous boreal summer (JJAS) La Niña forecast when the observed SST condition was neutral over NINO3.4 (Figure 1 *b*). The extreme ISMR departure in 1983 was captured only by February (L3) ICs, in magnitude and sign. To some extent, the departure of 1994 was also captured by CFSv2–NCEP L3. However, all ICs failed to forecast the departures of 1985, 1990, 1997, 1998 and 2006. The ISMR departures in CFSv2–NCEP were largely influenced by the sign and magnitude of their ENSO index forecasts; ISMR deficits were associated with El Niño or the anomalous warming of NINO3.4 SST, and excesses were associated with La Niña or the anomalous cooling of SSTs over the NINO3.4 region. The inverse relationship and interaction between ENSO and ISMR during boreal summer, have been well-documented[26–29]. This relationship is modulated on decadal timescales[30–34]. Most importantly, in CFSv2–NCEP reforecasts, ISMR was found to have over-sensitivity to ENSO, especially to SST fluctuation over the equatorial central Pacific region[35].

Further examination of yearly ISMR departures revealed that skill was not better in CFSv2–NCEP L3 compared to CFSv2–CSIR (Figure 1 *a*), though their correlations were 0.44 and 0.38 respectively. The difference between these two correlations was significant only at the 73% confidence level. However, previous studies have reported skill improvement in CFSv2 with February ICs with such differences in correlations for the ensemble means[14–17], though the exact correlation values varied from one study to another depending upon the region selected to average seasonal ISMR, the data used as reference/observation and duration of the analysis period.

In the case of observations, the ISMR departures of 1983, 1994, 1985, 1990, 1997, 1998 and 2006 were not strongly (and inversely) related to ENSO anomalies. The excesses of 1983 and 1990 were associated with neutral ENSO phases and those of 1994 and 2006 with mild warming and deficit of 1985 were associated with strong cooling over NINO3.4. In spite of strong El Niño in 1997 and La Niña in 1998, ISMR remained close to normal in observations. In comparison, ISMR departures of 1985, 1990, 1997, 1998 and 2006 were associated with very intense NINO3.4 SST anomalies in the model and both ICs we able to forecast the inverse ISMR departures. In other words, during these years the inverse relationship was strong and evident in the model, and ENSO was the dominant driving force determining the ISMR departure. Compared to observations, the model had a tendency to show amplified ENSO anomalies (skewed for cold events), more conspicuously for L3. For 1983 and 1994, larger errors were seen in ENSO predictions, with larger amplitudes in L3 reforecasts.

The correlation for CFSv2–NCEP L3 reduced to 0.4 if 1983 was excluded from the analysis period, which is lower than the corresponding score for CFSv2–CSIR Late-L1/Early-L0 ($\gamma = 0.42$) without 1983 (Figure 2). Similarly, the correlation for CFSv2–NCEP reforests with Late-L1/Early-L0 ICs increased from 0.35 to 0.45, when 1983 was excluded. It is to be noted that the ISMR departure of 1983 was captured only by L3 and not by Late-L1/Early-L0 (Figure 1 *a*), because of which the exclusion of 1983 decreased the correlation for L3 and increased it for Late-L1/Early-L0 ICs. Thus, the improved ISMR forecast skill of L3 was contributed by its successful prediction of 1983 ISMR excess. Next, we applied other deterministic verification scores such as mean error, bias and RMSE during the analysis period for assessing the forecast skill of CFSv2–NCEP L3 and CFSv2–CSIR Late-L1/Early-L0 (Table 1). These skill scores showed clear improvement in CFSv2–CSIR Late-L1/Early-L0 reforecasts compared to CFSv2–NCEP L3 (Table 1). For example, RMSE was lower in CFSv2–CSIR Late-L1/Early-L0 reforecasts. The deficiencies of CFSv2 such as underestimation of mean (dry bias) and standard deviation (SD; reduced variability) of ISMR, also improved and CV was closer to that observed in CFSv2–CSIR Late-L1/Early-L0.

Model intercomparison studies in the past have suggested that models which are skilful in representing climatological mean summer monsoon rainfall are more adept in simulating IAV of ISMR[36,37]. CFSv2 was found to have reasonable skill in capturing the spatial distribution of climatological JJAS mean rainfall, SST and 850 hPa winds over the Indian region (not shown). The
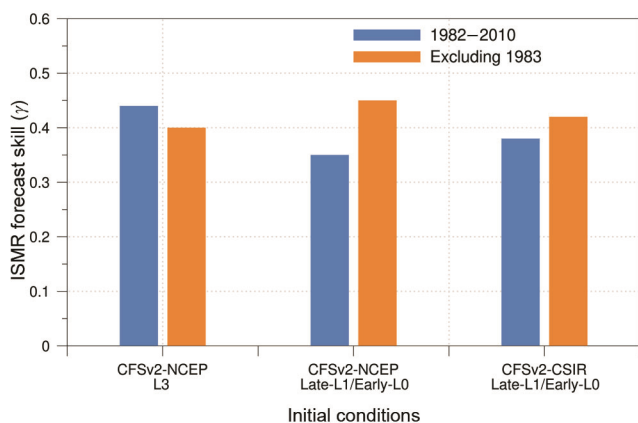

Figure 2. Correlation between standardized ISMR anomalies of IMD-based observations and ensemble mean of CFSv2–NCEP L3 reforecasts with February initial conditions (ICs) and CFSv2–NCEP and CFSv2–CSIR reforecasts with 5 Late-L1 (April)/Early-L0 (May) ICs for 1982–2010 and 1982–2010, excluding 1983.

Table 1. Skill scores for forecasting the interannual variation (IAV) of standardized (with standard deviation) anomalies of Indian summer monsoon rainfall (ISMR) averaged over the monsoon region by ensemble mean of CFSv2–NCEP L3 reforecasts and CFSv2–CSIR Late-L1/Early-L0 reforecasts, with respect to the corresponding India Meteorological Department (IMD) observations for the period 1982–2010. Time-series statistics against the observation, viz. mean error, bias and root-mean-square error are shown as the skill scores. The mean (μ), standard deviation (σ) and coefficient of variation (CV in %) of ISMR for the models and IMD observations are also given

IAV skill scores	CFSv2–NCEP L3 February initial conditions (ICs)	CFSv2–CSIR Late-L1/ Early-L0 April/May ICs	Observations (IMD)
Mean error (IAV)	–3.11	–1.99	
Bias (IAV)	0.64	0.69	
RMSE (IAV)	3.14	2.12	
ISMR μ (mm/day)	3.50	4.51	6.50
ISMR σ (mm/day)	0.51	0.66	0.76
ISMR CV (%)	14.5	10.3	11.7

mean rainfall bias was found to be lower in CFSv2–CSIR Late-L1/Early-L0 than in CFSv2–NCEP L3. Dry bias over India was larger in CFSv2–NCEP L3 compared to CFSv2–CSIR Late-L1/Early-L0. The pattern correlation coefficient (PCC), SD and mean bias were largely comparable among ensemble means of CFSv2–NCEP and CFSv2–CSIR reforecasts (not shown). However, the PCC was slightly larger for reforecasts with May ICs. SD and bias had clearly improved and the representation of mean monsoon rainfall over the Indian region was better in CFSv2–CSIR Late-L1/Early-L0 compared to CFSv2–NCEP L3. This is expected as atmospheric and oceanic states are close to JJAS. The increase in bias as lead time increases, indicates the role of dynamical drift in the model.

ISMR–ENSO relationship

The leading factor determining IAV of ISMR is the strong relationship between ISMR and ENSO in which there is an increased propensity of droughts during El Niño and of excess rainfall during La Niña[28]. It can be gleaned from Figure 1 that 8 out 12 excess events are associated with La Niña and 8 out of 12 deficit events are associated with El Niño in CFSv2–NCEP L3. There are no large excess events (large deficits) associated with El Niño (La Niña). All large excesses (large deficits) are associated with La Niña (El Niño). Thus, the ISMR–ENSO relationship is much stronger in CFSv2–NCEP L3 with a correlation of –0.85 between them, than in observations ($\gamma = -0.44$) where other factors influence ISMR (Figure 3). Correlation coefficients for the ensemble mean of CFSv2–NCEP reforecasts with L4, L2, L1, L0 and CFSv2–CSIR reforecasts with Late-L1/Early-L0 ICs are –0.86, –0.78, –0.85, –0.78 and –0.79 respectively. The strongest correlation for CFSv2–NCEP is seen for L4 followed by L3, and correlation is the lowest for L0 ICs. For CFSv2–CSIR Late-L1/Early-L0, the correlation is lower (–0.79) compared to L3. It is to be recalled that its ISMR forecast skill is also comparable with L3 for 1982–

2010, which becomes higher ($\gamma = 0.42$) than that of L3 ($\gamma = 0.40$) when 1983 is excluded from the analysis period (Figure 2). Thus, the correct forecast of 1983 ISMR excess by L3 occurred as a result of an erroneous La Niña forecast and contributed to the seemingly higher IAV correlation score for L3. However, other skill scores did not show higher ISMR forecast skill for L3 (Table 1). Moreover, the boreal summer ENSO forecast skill was found to be the lowest for L3 (Figure 1 b). This makes it necessary to analyse its ENSO forecast skill during boreal summer in detail.

Boreal summer ENSO forecast skill

CFSv2–NCEP L3 had serious deficiency in forecasting boreal summer-time ENSO (Figure 1 b). The forecast skill for JJAS ENSO index was found to be the lowest for CFSv2–NCEP L3 and L4 ($\gamma = 0.59$) compared to those for L2 to L0, and for CFSv2–CSIR Late-L1/Early-L0 ($\gamma = 0.76$). The verification of performance of CFSv2 in predicting the warm and cold SST anomalies over the NINO3.4 region was carried out based on the classification of hits, misses and false alarms in CFSv2–NCEP L3 and CFSv2–CSIR Late-L1/Early-L0 (not shown). The forecasts missed several events and there were few false alarms as well. The number of misses and false alarms for cold and warm events was found to be more for L3 forecasts. Thus, the performance was slightly better for CFSv2–CSIR Late-L1/Early-L0 in forecasting boreal summer ENSO index.

The forecast skill scores for June, July, August and September monthly ENSO indices against those observed during 1982–2010 (correlation coefficients given in Figures 4 a–d) indicate the bias in ENSO forecasts for L3. The forecast skill for the analysis period systematically dropped from June to September, with the least skill exhibited in September (Figure 4). During 1983, L3 predicted neutral condition in June and thereafter strong La Niña which kept intensifying from July to September. In contrast, in the case of observations, NINO3.4 had
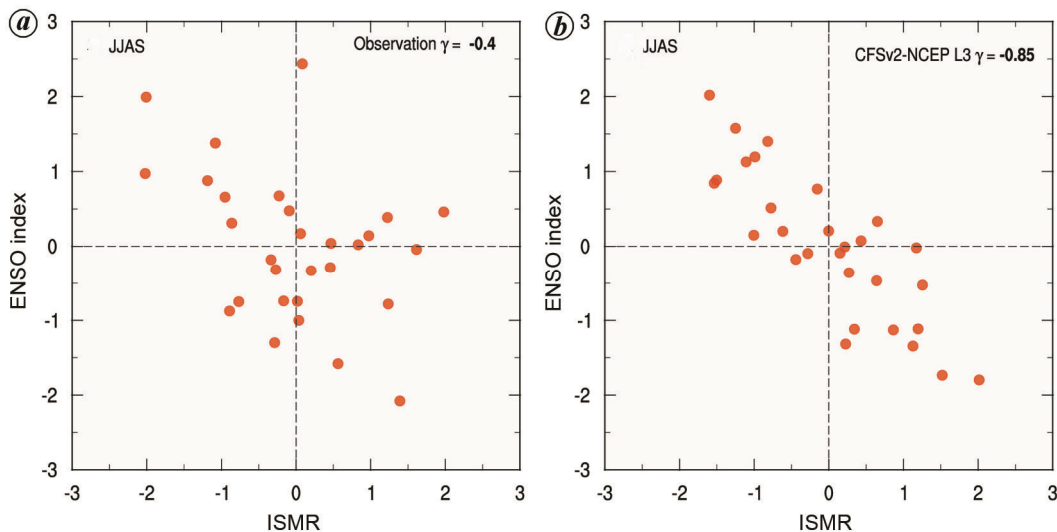
Figure 3. Anomalies of ISMR plotted against those corresponding to ENSO index during 1982–2010 for (**a**) observations and (**b**) CFSv2–NCEP L3 reforecasts. The respective correlation coefficients (γ) are given in the top-right.
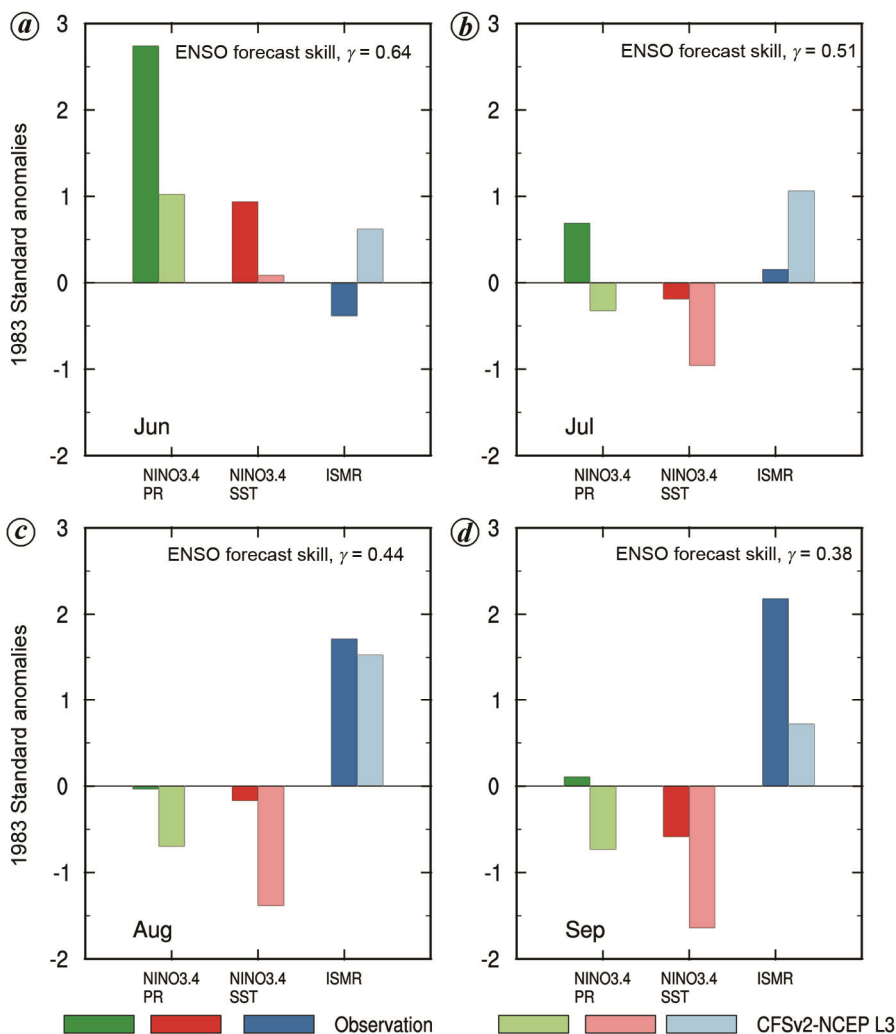

Figure 4. Monthly standardized anomalies of NINO3.4 rainfall (NINO3.4 PR) along with the corresponding anomalies of ENSO index (NINO3.4 SST) and ISMR from observations and ensemble mean of CFSv2–NCEP L3 reforecasts for (**a**) June, (**b**) July, (**c**) August and (**d**) September of 1983. The corresponding monthly ENSO forecast skill scores for June–September based on the correlation (γ) against the observed ENSO index during 1982–2010 are given at the top.

El Niño in June, neutral conditions in July and August, and a mild cold anomaly in September.

Correspondingly, the relationship of NINO3.4 SST with local NINO3.4 rainfall and remote impact on ISMR in 1983 showed model biases for L3. In the case of observations, there was enhanced NINO3.4 rainfall associated with El Niño in June, with a tendency to become normal as SSTs approached climatology and then develop into a cold anomaly by September. ISMR varied from below normal in June to normal in July, to large excesses in August and September. This was consistent with the inverse relationship between ISMR and ENSO. In L3, ENSO condition was very mild with anomalous rainfall over NINO3.4 in June, which dropped to strong La Niña in July and intensifies thereafter with deficit rainfall over NINO3.4. This resulted in above-normal ISMR in June and large excesses in July to September of 1983.

The strong association of local rainfall with NINO3.4 SST, even with cold bias over the equatorial Pacific Ocean in CFSv2 (not shown), can be understood from the SST–rainfall relationship over NINO3.4 during June to September of 1982–2010. Figure 5 shows the variation of mean rainfall with SST for each 0.25°C SST and 0.5 mm/day rainfall bin. The observed relationship ($\gamma = 0.59$) shows that the rainfall steadily increases with SST from about 27°C with high propensity of rainfall for SSTs above this threshold. In CFSv2–NCEP L3, the slope of the curve is steeper than that observed, and there is a slight shift in the SST–rainfall relationship towards colder SSTs. This is also consistent with the finding that the SST–rainfall pattern in coupled models is similar to the corresponding observation or atmosphere-only version, except for a shift in pattern to colder/warmer SSTs according to their seasonal mean cold/warm bias[38].
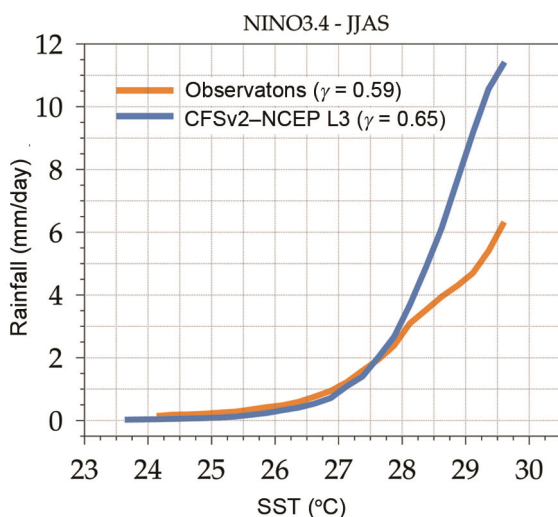
Role of bias in SST boundary forcing

In CFSv2, the SST–rainfall association/relationship over NINO3.4 was stronger with a correlation of 0.65 than that observed (Figure 5), which in turn seems to have a remote impact on ISMR. Thus the ISMR prediction depends significantly on ENSO. This indirectly implies that the reduction of SST bias over central Pacific can contribute to improvement in ISMR forecast skill. Further, the variation of daily SST averaged over the NINO3.4 region shows that SST starts falling sharply after the beginning of the monsoon season in 1983 (Figure 6). The fall in SST is steep and large. In 1983, the corresponding CFSv2–NCEP forecasts with L0 (May) and Late-L1/Early-L0 ICs showed lesser cooling. The characteristics of the evolution of 1983 SST over NINO3.4 for Late-L1/Early-L0 ICs remained the same in the current version of CFSv2 as well. The build-up of bias hints at the role of dynamic drift and model bias resulting in much colder SSTs leading to La Niña by the summer months for L3. Given the high sensitivity of ISMR to NINO3.4 SST boundary forcing, a systematic approach to minimize SST bias is essential to achieve the potential predictability.

Equatorial Indian Ocean

Another mode of SST variability in the equatorial IO is the occurrence of opposite SST anomalies over eastern

Figure 5. Variation of mean rainfall versus mean SST for each 0.25°C SST and 0.5 mm/day rainfall bin from observations (orange curve) and ensemble mean of CFSv2–NCEP L3 reforecasts (blue curve) showing the relationship between rainfall and SST over NINO3.4, during June–September of 1982–2010.
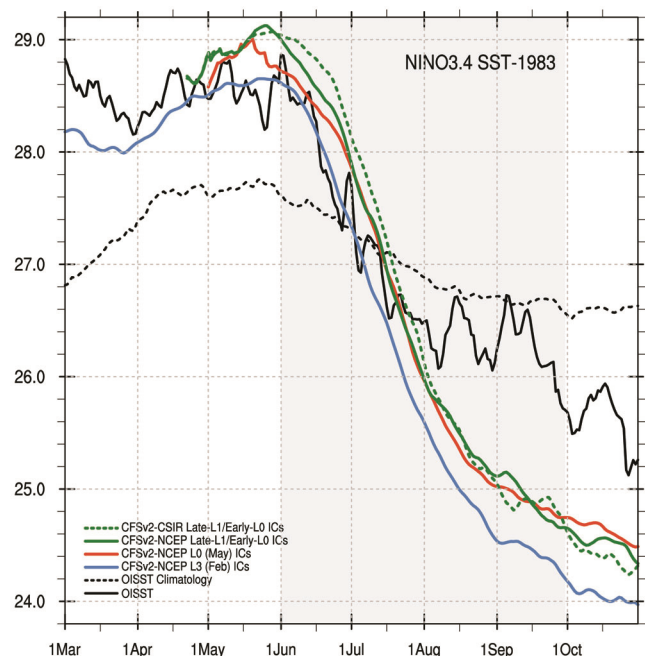
Figure 6. Temporal evolution of daily SST averaged over NINO3.4 from optimum interpolation SST (OISST) observations, OISST daily long-term climatology and ensemble mean of CFSv2–NCEP reforecasts with L3 (February), L0 (May) and Late-L1 (April)/Early-L0 (May) ICs and ensemble mean of CFSv2–CSIR reforecasts with Late-L1/Early-L0 ICs.

equatorial IO (EEIO, 90°–110°E; 10°S–0°N) and western equatorial IO (WEIO, 50°–70°E; 10°S-10°N), known as the Indian Ocean dipole (IOD)[39]. Climatologically, IO is warmer in the east supporting more convection than in the west during monsoon. The positive IOD phase is characterized by weakening or reversal of climatological zonal SST gradient with suppression (enhancement) of convection over east (west) and anomalous winds blow from east to west along the equator, lifting the thermocline and mixed layer of the east. However, the relationship between ISMR and IOD during JJAS was found to be rather weak, with the correlation coefficient not significantly different from zero, and only about 1% of ISMR variance explained by IOD[40].

The atmospheric counterpart of IOD, the EQUINOO, with its positive (negative) phase associated with enhanced convection over WEIO (EEIO) and suppressed convection over EEIO (WEIO) is found to play an important role in determining IAV of ISMR[22] with the positive (negative) phase favourable (unfavourable) for ISMR. As the positive (negative) EQUINOO phase is associated with an easterly (westerly) anomaly of the zonal wind over the central equatorial IO, the EQUINOO index is based on the surface zonal wind anomaly over this region. Although EQUINOO is considered to be the atmospheric component of the coupled IOD mode, unlike ENSO, it is not as tightly coupled[40], with the correlation between the indices being only ~0.45.

Spatial distribution of observed anomalies of rainfall, SST and winds in 1983 showed that the enhanced rainfall over India was due to a positive EQUINOO (convective WEIO), whereas in CFSv2–NCEP L3, it was associated with La Niña (not shown). In CFSv2–CSIR Late-L1/Early-L0, ISMR deficit was associated with El Niño. Both forecasts did not show the important positive association between monsoon rainfall over WEIO and the Indian region. Further analysis revealed that in CFSv2, EQUINOO appeared to occur due to the impact of ENSO on the equatorial IO. The impact of El Niño resulted in warming and enhancement of rainfall over WEIO, and cooling and suppression of rainfall over the EEIO region extending up to the West Pacific and over the Indian region. During La Niña, opposite impacts occurred over WEIO, EEIO and the Indian region. Thus, ENSO elicits an inverse relationship between WEIO and EEIO, which is analogous to the EQUINOO characteristics over the equatorial IO. The ENSO impact results in an inverse relationship between ISMR and WEIO rainfall, which is in contrast to their observed relationship associated with EQUINOO. The fact that enhanced cross-equatorial flow is associated with increased moisture transport and enhanced off-equatorial diabatic heating along the monsoon convergence zone over India results in strong positive correlation between convection over WEIO and ISMR, which is observed during strong EQUINOO events. However, CFSv2 fails to capture this important

relationship. In contrast, 'EQUINOO-like' events with opposite poles of anomalies of SST, rainfall and circulation over equatorial WEIO and EEIO occur which are induced by ENSO in the model (not shown). This is associated with an opposite relationship between WEIO convection and ISMR.

In CFSv2, ENSO and EQUINOO resulted in reinforcing each other's inverse impact on ISMR, in contrast to observations, where they were either independent or tend to oppose each other. This leads to much stronger than the observed inverse relationship between ENSO and ISMR in CFSv2 (ref. 35; Figures 3 and 4). Correspondingly, ENSO and EQUINOO showed an intense correlation between them; 0.83 in CFSv2–NCEP L3 (which is the largest among ICs, Figure 7 b) and 0.58 in CFSv2–CSIR Late-L1/Early-L0. The correlation coefficients (γ) for CFSv2–NCEP reforecasts with L4, L2, L1 and L0 ICs were 0.79, 0.81, 0.72 and 0.59 respectively. In contrast, in the case of observations they were almost independent ($\gamma = 0.14$, Figure 7 a). Thus, the ISMR–EQUINOO relationship was also strong and opposite to the observed relationship ($\gamma = 0.54$, Figure 7 c) in CFSv2–NCEP L3 ($\gamma = -0.77$, Figure 7 d). The corresponding correlation coefficients for CFSv2–NCEP reforecasts with L4, L2, L1 and L0 ICs were –0.71, –0.71, –0.67 and –0.44 respectively. Thus the largest negative correlation was for CFSv2–NCEP L3. The relationship was opposite to that observed in CFSv2–CSIR Late-L1/Early-L0 as well, but with slightly weaker correlation of –0.56 than L3.

Forecasting of the 1994 ISMR departure by L3 was also due to an erroneous La Niña forecast, when in reality ISMR was in excess only due to positive EQUINOO (shown by '+' in Figure 1 a and b). In CFSv2, ISMR departure was almost entirely decided by ENSO, whereas in the case of observations EQUINOO was found to play a decisive role during several years (Figure 1). The excesses of 1983 (with neutral ENSO condition), and 1994 and 2006 (with mild warm ENSO anomalies) were also due to positive EQUINOO events (Figure 1). Similarly, ISMR of 1985 was below normal due to negative EQUINOO despite having a strong cold ENSO anomaly. Normal monsoons of 1997 and 1998 were due to positive and negative EQUINOO events, despite having strong El Niño and La Niña respectively. CFSv2 showed little skill in forecasting EQUINOO, where the correlation between observed and predicted anomalies of the EQUINOO index for 1982–2010 was –0.14 (0.16) for CFSv2–NCEP L3 (CFSv2–CSIR Late-L1/Early-L0). The inability of CFSv2 to forecast EQUINOO events correctly and independent of ENSO made it impossible for the model to forecast ISMR anomalies of 1985, 1990, 1997, 1998 and 2006 with almost all ICs.

The major ISMR departures were either inversely related to ENSO and/or positively related to EQUINOO in the observations (Figure 1). In CFSv2, most of the ISMR departures were negatively correlated to both
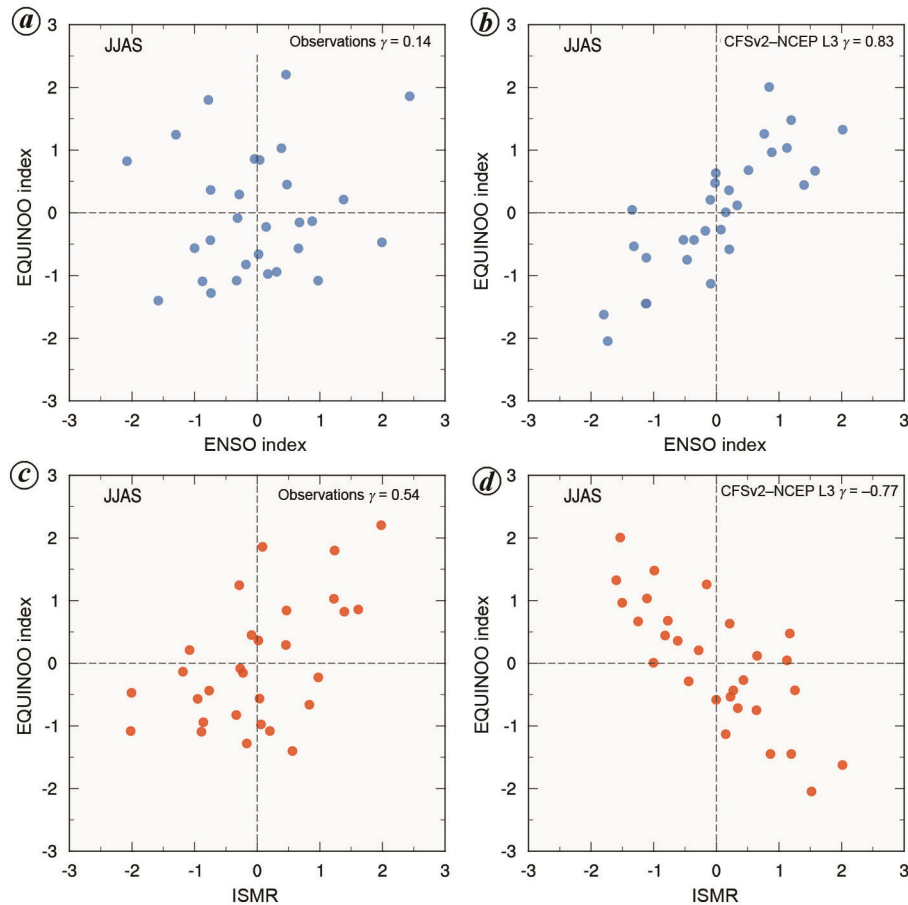
Figure 7. Anomalies of ENSO index plotted against the corresponding anomalies of EQUINOO index for (*a*) observations and (*b*) CFSv2–NCEP L3 reforecasts. Anomalies of ISMR plotted against their corresponding to EQUINOO index for (*c*) observations and (*d*) CFSv2–NCEP L3 reforecasts.

ENSO and EQUINOO. For example, in 1983, CFSv2–NCEP L3 (CFSv2–CSIR Late-L1/Early-L0) predicted excess (below normal) ISMR associated with La Niña (El Niño) and negative (neutral) EQUINOO. The variation of observed daily SST averaged over WEIO (Figure 8 *a*) and EEIO (Figure 8 *b*) showed that SSTs were warmer than normal over WEIO and remained near-normal or slightly colder than normal over EEIO during the monsoon season of 1983. These are the typical characteristics of the positive phase of EQUINOO which resulted in ISMR excess in the presence of near-neutral ENSO conditions over the NINO3.4 region in the observations (Figure 6). However, in CFSv2, WEIO was much colder than normal during the monsoon season, with L3, L0 and Late-L1/Early-L0 ICs, which is the characteristic of the negative phase of EQUINOO. Correspondingly, SSTs over EEIO remained warmer than normal in CFSv2–NCEP L3 as seen during the negative EQUINOO phase. In contrast, SSTs over EEIO were much colder in CFSv2 with L0 and Late-L1/Early-L0 ICs reducing the east–west SST gradient and EQUINOO for the monsoon season turning out to be neutral for these ICs (also shown in Figure 1 for 1983 of

CFSv2–CSIR Late-L1/Early-L0). It is to be noted that CFSv2–NCEP L3 predicts La Niña, which results in cooling (warming) of WEIO (EEIO) and leads to excess ISMR in 1983. On the contrary, CFSv2 with L0 and Late-L1/Early-L0 ICs predicts warmer than normal SSTs over the NINO3.4 region for the first part of the monsoon season (Figure 6) along with neutral EQUINOO leading to below-normal ISMR in 1983. This demonstrates that the ISMR excess of 1983 is primarily due to the wrong forecast of La Niña over the NINO3.4 region (which leads to wrong EQUINOO forecast as well) by CFSv2–NCEP L3. Our analysis thus reveals that ENSO is the major decisive factor for anomalies of ISMR and also EQUINOO in CFSv2, and this deficiency is larger in reforecasts with L3 ICs. Initiating seasonal forecasts from Late-L1/Early-L0 ICs can yield slightly improved forecasts.

Concluding remarks

This study analyses the factor which contributes to the highest ISMR forecast skill for February (three-month
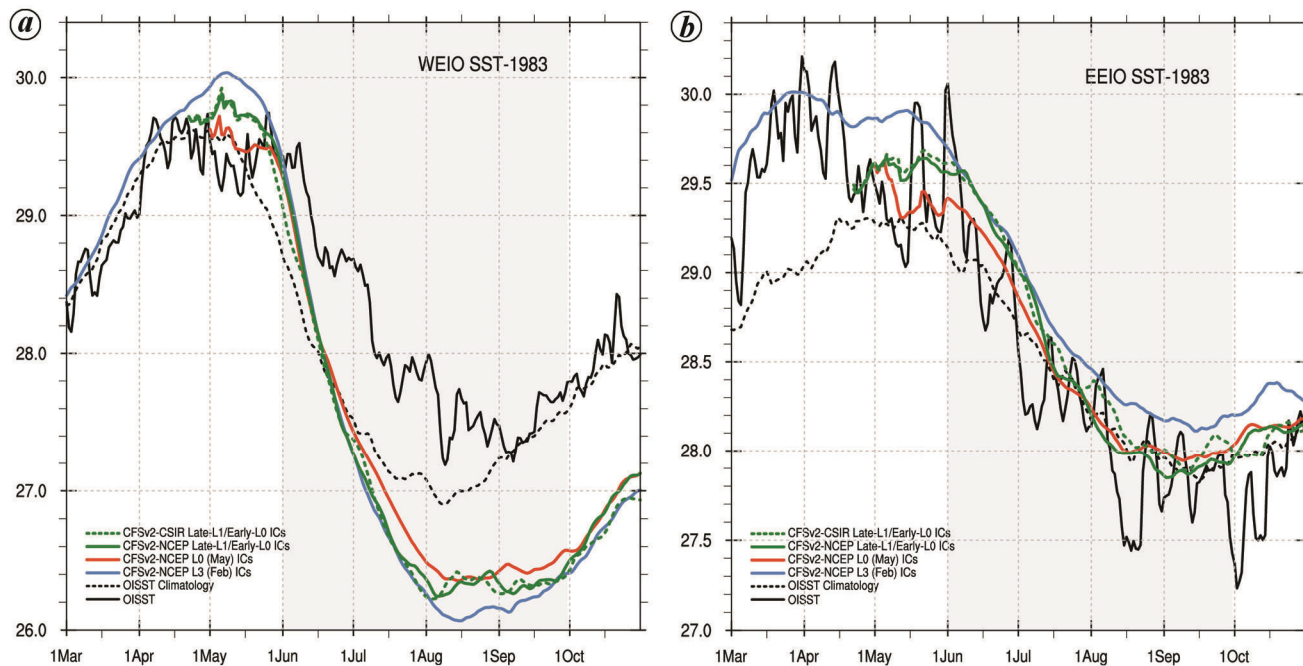
Figure 8. *a*, Temporal evolution of daily SST averaged over the western equatorial Indian Ocean (WEIO, 50°–70°E; 10°S–10°N) from Optimum Interpolation Sea Surface Temperature (OISST) observations, OISST daily long-term climatology and ensemble mean of CFSv2–NCEP reforecasts with L3 (February), L0 (May) and Late-L1 (April)/Early–L0 (May) ICs and ensemble mean of CFSv2–CSIR reforecasts with Late-L1/Early-L0 ICs. *b*, Same as (*a*), but for daily SST averaged over the eastern equatorial Indian Ocean (EEIO, 90°E–110°E; 10°S–0°).

forecast lead time, L3) ICs in CFSv2, as reported in previous studies. We analysed nine-month retrospective reforecasts by CFSv2 initiated from January (four-month forecast lead time, L4) through May (0-month forecast lead time, L0) ICs, provided by NCEP for 1982–2010 (referred to as CFSv2–NCEP reforecasts). Our analysis revealed that the reported higher forecast skill for February (L3) ICs is based on a single skill score of correlation between observed and predicted ISMR departures during the analysis period. In contrast, other skill scores such as the mean error, interannual bias, RMSE, climatological summer mean rainfall and SD and CV of ISMR indicate higher or comparable forecast skill for April/May (L1/L0) ICs. Climatological bias in mean summer monsoon rainfall over India was also found to be the least with L1/L0 ICs. These results were reconfirmed through the analysis of a set of experimental reforecasts by the current version of CFSv2 with an optimum subset of five late-April/early-May (Late-L1/Early-L0) ICs which had shorter yet useful forecast lead times (referred to as CFSv2–CSIR Late-L1/Early-L0). Correspondingly, reforecasts with Late-L1/Early-L0 ICs yielded a correlation skill score comparable to that of L3 and the deterministic ISMR forecast skill was found to be the best with Late-L1/Early-L0 ICs for 1982–2010 period, if 1983 was excluded.

The success of CFSv2–NCEP L3 in forecasting a single event, i.e. excess ISMR departure in 1983, contributed to its higher IAV correlation score of 0.44. The cor-

relation was 0.38 for CFSv2–CSIR late-April/early-May ICs, which is not significantly different from that of CFSv2–NCEP L3. These correlations were 0.40 and 0.42 for CFSv2–NCEP L3 and CFSv2–CSIR respectively, if 1983 was excluded from the analysis period of 1982–2010. Further, we found that the success of CFSv2–NCEP L3 in forecasting the 1983 ISMR excess was due to its wrong forecast of La Niña (unlike April (L1) and May (L0) ICs) during the boreal summer of 1983. Our analysis thus suggests the importance of initializing seasonal forecasts from April/May ICs.

The common deficiencies of CFSv2 such as the over-intensified influence of ENSO on ISMR and on variation of SST, rainfall and circulation over the equatorial IO, are also important factors which contribute to errors in ISMR forecasting. In CFSv2, ISMR is almost entirely decided by ENSO-related SST boundary forcing, with no link between variabilities of ISMR and convection over the equatorial IO associated with EQUINOO. In contrast, in the observations, ISMR is influenced by both ENSO and EQUINOO independently.

The central Pacific was under the sway of El Niño till June 1983. All forecasts were initiated when El Niño prevailed with active convection over NINO3.4. CFSv2 is known to develop pronounced wet and cold bias over the central Pacific. The fact that CFSv2–NCEP L3 with long lead time ended in forecasting La Niña in summer hints at the possible role of wet bias and associated winds resulting in stronger cooling of NINO3.4 ocean surface for L3.

This also implies that the persistence of errors in atmospheric circulation due to imperfections in physical processes could eventually lead to large-scale bias in ocean circulation and surface temperatures. This can be manifested in larger magnitudes in forecasts with longer lead times. Improvements in atmospheric model physics schemes and experiments with observed SST forced atmosphere-only component of CFSv2 can throw further light on these aspects. It is also important to determine if the ocean model of CFSv2 can simulate oceanic modes correctly when forced with realistic atmospheric circulation and fluxes. Our analysis suggests the need for a systematic approach to minimize the biases in SST boundary forcing in CFSv2, to achieve improved ISMR forecasts.

Appendix 1. Forecast skill scores

The scores used for verifying the skill of forecasts are the following:

1. Mean error is average error.

$$\text{Mean error} = \frac{1}{N}\sum_{i=1}^{N}(F_i - O_i)$$

where F_i and O_i are the predicted and observed Indian summer monsoon rainfall (ISMR) for the ith year and N is the number of years.

2. Bias is a comparison of average forecast magnitude to that observed.

$$\text{Bias} = \frac{\frac{1}{N}\sum_{i=1}^{N}F_i}{\frac{1}{N}\sum_{i=1}^{N}O_i}.$$

3. Root-mean-square error (RMSE) is the average magnitude of forecast errors.

$$\text{RMSE} = \sqrt{\frac{1}{N}\sum_{i=1}^{N}(F_i - O_i)^2}.$$

4. In addition, the amount of climatological JJAS rainfall over the Indian land region (μ), the corresponding standard deviation of JJAS mean rainfall (σ) and its temporal coefficient of variation (CV; %) for 1982–2010 are estimated as:

$$\mu = \frac{\sum_{i=1}^{N}\text{India rainfall}_{(\text{JJAS})_i}}{N},$$

$$\sigma = \sqrt{\frac{\sum_{i=1}^{N}(\text{India rainfall}_{(\text{JJAS})_i} - \mu)^2}{N}},$$

$$\text{CV} = \frac{\sigma}{\mu} \times 100.$$

1. DelSole, T. and Shukla, J., Climate models produce skillful predictions of Indian summer monsoon rainfall. *Geophys. Res. Lett.*, 2012, **39**, L09703; doi:10.1029/2012GL051279.
2. Saha, S. *et al.*, The NCEP climate forecast system reanalysis. *Bull. Amer. Meteorol. Soc.*, 2010, **91**, 1015–1057.
3. Krishnamurthy, V. and Rai, S., Predictability of South Asian monsoon circulation in the NCEP climate forecast system. *Adv. Geosci.*, 2011, **22**, 65–76.
4. Pattanaik, D. R., Mukhopadhyay, B. and Kumar, A., Monthly forecast of Indian southwest monsoon rainfall based on NCEP's coupled forecast system. *Atmos. Climate Sci.*, 2012, **2**(4), 479–491.
5. Saha, S. *et al.*, The NCEP climate forecast system version 2. *J. Climate*, 2014, **27**, 2185–2208.
6. Pattanaik, D. R. and Kumar, A., Prediction of summer monsoon rainfall over India using the NCEP climate forecast system. *Climate Dyn.*, 2010, **34**, 557–572.
7. Charney, J. G. and Shukla, J., Predictability of monsoons. *Monsoon Dyn.*, 1981, **4**, 99–109.
8. Rasmusson, E. M. and Carpenter, T. H., The relationship between eastern equatorial Pacific sea surface temperatures and rainfall over India and Sri Lanka. *Mon. Weather Rev.*, 1983, **111**(3), 517–528.
9. Shukla, J. and Wallace, J. M., Numerical simulation of the atmospheric response to equatorial Pacific sea surface temperature anomalies. *J. Atmos. Sci.*, 1983, **40**, 1613–1630.
10. Krishnamurthy, V. and Shukla, J., Predictability of the Indian monsoon in coupled general circulation models. COLA Tech. Rep., 2011, no. 313.
11. Slingo, J. and Palmer, T. N., Uncertainty in weather and climate prediction. *Philos. Trans. R. Soc. London Ser.*, 2011, **369**, 4751–4767.
12. Kumar, A., Chen, M. and Wang, W., An analysis of prediction skill of monthly mean climate variability. *Climate Dyn.*, 2011, **37**(5), 1119–1131.
13. Webster, P. J. and Yang, S., Monsoon and ENSO: selectively interactive systems. *Q. J. R. Meteorol. Soc.*, 1992, **118**, 877–926.
14. Pokhrel, S. *et al.*, Seasonal prediction of Indian summer monsoon rainfall in NCEP CFSv2: forecast and predictability error. *Climate Dyn.*, 2016, **46**, 2305–2326.
15. Ramu, D. A. *et al.*, Indian summer monsoon rainfall simulation and prediction skill in the CFSv2 coupled model: impact of atmospheric horizontal resolution. *J. Geophys. Res. Atmos.*, 2016, **121**(5), 2205–2221.
16. Pillai, P. A. *et al.*, Seasonal prediction skill of Indian summer monsoon rainfall in NMME models and monsoon mission CFSv2. *Int. J. Climatol.*, 2018, **38**, e847–e861.
17. Rao, S. A. *et al.*, Monsoon Mission: a targeted activity to improve monsoon prediction across scales. *Bull. Am. Meteorol. Soc.*, 2019, **100**(12), 2509–2532.
18. Schaeybroeck, B. V. and Vannitsem, S., Postprocessing of long-range forecasts. In *Statistical Postprocessing of Ensemble Forecasts*, Elsevier, 2019, chapter 10, pp. 267–290.
19. Pai, D. S., Latha, S., Rajeevan, M., Sreejith, O. P., Satbhai, N. S. and Mukhopadhyay, B., Development of a new high spatial resolution (0.25° × 0.25°) long period (1901–2010) daily gridded rainfall data set over India and its comparison with existing data sets over the region. *Mausam*, 2014, **65**, 1–18.
20. Adler, R. F. *et al.*, The version 2 Global Precipitation Climatology Project (GPCP) monthly precipitation analysis (1979–present). *J. Hydrometeorol.*, 2003, **4**, 1147–1167.
21. Rayner, N. A. *et al.*, Global analyses of SST, sea ice and night marine air temperature since the late nineteenth century. *J. Geophys. Res.: Atmos.*, 2003, **108**, 4407; 10.1029/2002JD002670.
22. Reynolds, R. W., Smith, T. M., Liu, C., Chelton, D. B., Casey, K. S. and Schlax, M. G., Daily high-resolution blended analyses for sea surface temperature. *J. Climate*, 2007, **20**, 5473–5496.

23. Hersbach, H. *et al.*, The ERA5 global reanalysis. *Q. J. R. Meteorol. Soc.*, 2020, **146**(730), 1999–2049.

24. Gadgil, S., Vinayachandran, P. N., Francis, P. A. and Gadgil, S., Extremes of Indian summer monsoon rainfall, ENSO, equatorial Indian Ocean oscillation. *Geophys. Res. Lett.*, 2004, **31**, L12213.

25. Gadgil, S., Rajendran, K. and Pai, D. S., A new rain-based index for the Indian summer monsoon rainfall. *Mausam*, 2019, **70**(30), 485–500.

26. Walker, G. T. and Bliss, E. W., World weather. *Mem. R. Meteorol. Soc.*, 1932, **4**, 53–84.

27. Walker, G. T., Seasonal weather and its prediction. *Nature*, 1933, **132**(3343), 805–808.

28. Sikka, D. R., Some aspects of the large-scale fluctuations of summer monsoon rainfall over India in relation to fluctuations in the planetary and regional scale circulation parameters. *Proc. Indian Acad. Sci. (Earth Planet. Sci.)*, 1980, **89**, 179–195.

29. Torrence, C. and Webster, P. J., Interdecadal changes in the ENSO-monsoon system. *J. Climate*, 1999, **12**(8), 2679–2690.

30. Kumar, K. K., Rajagopalan, B. and Cane, M. A., On the weakening relationship between the Indian monsoon and ENSO. *Science*, 1999, **284**(5423), 2156–2159.

31. Chen, W., Dong, B. and Lu, R., Impact of the Atlantic Ocean on the multidecadal fluctuation of El Niño-southern oscillation–south Asian monsoon relationship in a coupled general circulation model. *J. Geophys. Res.*, 2010, **115**, D17109.

32. Kumar, K. K., Rajagopalan, B., Hoerling, M., Bates, G. and Cane, M. A., Unraveling the mystery of Indian monsoon failure during El Niño. *Science*, 2006, **314**(5796), 115–119.

33. Azad, S. and Rajeevan, M., Possible shift in the ENSO–Indian monsoon rainfall relationship under future global warming. *Sci. Rep.*, 2016, **6**(1), 20145.

34. Fan, F. *et al.*, Revisiting the relationship between the South Asian summer monsoon drought and El Niño warming pattern. *Atmos. Sci. Lett.*, 2017, **18**(4), 175–182.

35. Vishnu, S., Francis, P. A., Ramakrishna, S. S. V. S. and Schenoi, S. S. C., On the relationship between the Indian summer monsoon rainfall and the EQUINOO in the CFSv2. *Climate Dyn.*, 2019, **52**, 1263–1281.

36. Sperber, K. R. and Palmer, T. N., Interannual tropical rainfall variability in general circulation model simulations associated with the Atmospheric Model Intercomparison Project. *J. Climate*, 1996, **9**, 2727–2750.

37. Gadgil, S. and Sajani, S., Monsoon precipitation in the AMIP runs. *Climate Dyn.*, 1998, **14**, 659–689.

38. Rajendran, K., Nanjundiah, R. S., Gadgil, S. and Srinivasan, J., How good are the simulations of tropical SST–rainfall relationship by IPCC AR4 atmospheric and coupled models? *J. Earth Syst. Sci.*, 2012, **121**(3), 595–610.

39. Saji, N. H., Goswami, B. N., Vinayachandran, P. N. and Yamagata, T., A dipole in the tropical Indian Ocean. *Nature*, 1999, **401**, 360–363.

40. Sajani, S., Gadgil, S., Francis, P. A. and Rajeevan, M., Prediction of Indian rainfall during the summer monsoon season on the basis of links with equatorial Pacific and Indian Ocean climate indices. *Environ. Res. Lett.*, 2015, **10**, 094004.